Engineering Fracture Mechanics 227 (2020) 106733

Contents lists available at ScienceDirect

Engineering Fracture Mechanics

journal homepage: www.elsevier.com/locate/engfracmech

Studying the interaction of crack-like flaws using the MATLAB toolbox int_defects

H.E. Coules*, M.A. Probert

Department of Mechanical Engineering, University of Bristol, Bristol BS8 1TR, UK

ARTICLE INFO

Keywords:
Finite element analysis
Fracture mechanics
Limit load
Flaw interaction

ABSTRACT

int_defects is a free and open-source toolbox for MATLAB which uses the Abaqus finite element analysis suite to automate the analysis of interacting crack-like flaws in structures. It is designed to aid the development of flaw interaction criteria for structural integrity assessment procedures and to simplify sensitivity analysis of flaw proximity. It can also perform automatic 3D elastic, elastic-plastic or limit load analysis of elliptical embedded flaws and semi-elliptical surface flaws in plates and thick-walled pipes under a wide range of loading conditions. This technical note outlines the capabilities of int_defects and gives some examples of its use.

1. Introduction

Finite Element Analysis (FEA) can be used to investigate structures containing crack-like flaws. Typically, this type of investigation is motivated by a need to predict the initiation or progress of fracture, fatigue or ductile tearing from a pre-existing structural defect. The crack-driving force that results from a known structural loading state is determined using FEA and then compared with the material's fracture toughness properties to predict whether or not the crack will extend.

Compendia of functions which relate the load applied to a structure containing a crack-like flaw to the crack tip Stress Intensity Factor (SIF) or J-integral, or the structure's plastic limit load, are used widely in practical fracture-mechanics-based analysis of structural integrity [1]. These pre-calculated functions are normally based on numerical modelling results, often with experimental validation for selected cases. In the Failure Assessment Diagram (FAD) approach, which forms the basis of general-purpose structural integrity assessment procedures such as BS 7910 [2] and R6 [3], compendia of SIF and limit load solutions are used to minimise the need to perform numerical modelling of structures containing crack-like flaws on a case-by-case basis.

Most modern FEA pre-processors such as Abaqus/CAE [4] can generate large-scale 3-dimensional meshes automatically, which makes it feasible to consider many different geometries and loading conditions in a parametric set of cracked-body analyses. Since the late 1980s, specialised packages for pre- and post-processing of FE models of fracture have also emerged, often incorporating special-purpose meshing algorithms. These include FEACrack (Quest Integrity USA LLC, USA) [5], Zencrack (Zentech International Ltd., UK) [6] and FRANC3D (Fracture Analysis Consultants Inc., USA) [7]. The Dual Boundary Element Method (DBEM) [8,9] has also frequently been used to determine the crack driving force in parametric studies which involve multiple crack geometries and loading conditions, sometimes using hybrid FEM-DBEM sub-modelling schemes [10].

One common complication in structural integrity analysis the possibility of multiple structural defects occurring close to one another [11]. If the defects are close enough to interact then the effect of this interaction should be considered carefully when judging the structure's fitness-for-service. On the other hand, if it can be shown that each defect has a negligible effect on the other then each

* Corresponding author.
E-mail address: harry.coules@bristol.ac.uk (H.E. Coules).

https://doi.org/10.1016/j.engfracmech.2019.106733
Received 3 July 2019; Received in revised form 3 October 2019; Accepted 14 October 2019
Available online 25 October 2019

Nomenclature

a	Flaw depth
b	Plate thickness (or pipe wall thickness)
c	Flaw half-width
d	Inter-flaw spacing
d_2	Embedded flaw depth below surface
E	Young's modulus
$J_{0.2}$	Elastic-plastic fracture toughness (at 0.2 mm of crack growth)
K_I	Mode I Stress Intensity Factor
K_I^{int}	Mode I Stress Intensity Factor at a flaw in an interacting pair
$K_I^{\delta=\infty}$	Mode I Stress Intensity Factor at a remotely-located flaw
n	Ramberg-Osgood hardening coefficient
n_{GL}	Global limit load
p_{LL}	Local limit pressure
p_{UL}	Limit pressure for an unflawed pipe
Q	Shape factor of an elliptical/semi-elliptical flaw
r_i	Pipe internal radius
r_o	Pipe external radius
W	Plate half-width
y_{off}	Through-thickness offset distance of an embedded flaw
α	Ramberg-Osgood yield offset parameter
α_1	Normalised flaw depth ($\frac{a}{b}$)
γ	Elastic interaction factor
ε	Strain
η_i	Pipe wall thickness parameter ($\frac{b}{r_i}$)
ν	Poisson's ratio
σ	Stress
σ_{VM}	von Mises' stress component
σ_Y	Yield stress
ϕ	Ellipse parametric angle
Φ	Flaw aspect ratio ($\frac{a}{c}$)

Abbreviations

FAD	Failure Assessment Diagram
FE(A)	Finite Element (Analysis)
LLL	Local Limit Load
MLOCA	Medium Loss-Of-Coolant Accident
RAM	Random Access Memory
RPV	Reactor Pressure Vessel
SIF	Stress Intensity Factor

one can be considered in isolation. Consequently, integrity assessment procedures often contain criteria for predicting whether multiple defects will interact and rules specifying how the analysis should proceed if the interaction is judged to be significant, e.g. by re-characterising multiple flaws as a single, enclosing flaw [12–14]. A comparison of several interaction criteria for co-planar flaws is given by Hasegawa & Miyazaki [15].

Formulating defect interaction criteria and recharacterisation rules is challenging because the range of possible situations that may occur in any individual assessment (in terms of defect sizes, shapes, spacings, loading states and failure mechanisms) is very broad. Any general interaction criterion must be valid for a wide range of different cases, so validation requires many experiments or models. Over the last three decades, schemes for parametric analysis of interacting flaws have been developed and refined [16–18]. This technical note outlines a method for performing large-scale parametric analysis of interacting crack-like flaws. The method has been used in several previous studies [19–23], and has now been implemented in the free and open-source "int_defects" toolbox for MATLAB [24] which interfaces with the Abaqus FEA package [4,25]. int_defects is designed for analysing the interaction of co-planar elliptical embedded flaws and semi-elliptical surface flaws in plates and thick-walled pipes. It supports arbitrary flaw dimensions, loading states and material stress-strain characteristics.

2. The MATLAB toolbox int_defects

2.1. Description and capabilities

int_defects can determine SIFs, J-integrals and plastic limit loads for single semi-elliptical surface cracks and elliptical embedded cracks of arbitrary size/shape in a plate or pipe of finite thickness, as well as co-planar pairs of such cracks. It is designed to automate the generation, execution and post-processing of large sets of FE models which contain different crack geometries and loading states. int_defects includes functions for post-processing elastic-plastic model results to collate crack tip J-integral values. The J-integral is initially determined by the Abaqus/Standard FE solver using an equivalent domain integral [26] and in elastic analyses the Mode I SIF is calculated from the J-integral using the interaction integral method [27]. Both J-integral and SIF results can be checked for path-independence automatically using the toolbox. int_defects also post-processes elastic → perfectly-plastic model results to determine plastic limit loads. For example, int_defects can automatically determine the Local Limit Load (LLL), i.e. the load at which a plastic ligament forms between a crack and the back face of the section. The LLL is significant for structural integrity assessment and is used in the FAD approach to conservatively estimate a flawed structure's proximity to plastic collapse [1,28].

In post-processing, int_defects can compare results from a set of linear elastic models of single cracks with those from models of paired cracks, to determine the degree of stress interaction between the cracks in proximity. The elastic interaction factor (γ) can be calculated as:

$$\gamma(\phi) = \frac{K_I^{int}(\phi)}{K_I^{\delta=\infty}(\phi)} \tag{1}$$

where K_I^{int} is the SIF at a flaw that is part of an interacting pair and $K_I^{\delta=\infty}$ is the SIF for the same flaw in isolation. K_I^{int}, $K_I^{\delta=\infty}$ and γ are

all functions of position on the crack tip line, which is defined using the ellipse parametric angle ϕ.

int_defects is designed for analysing co-planar pairs of cracks in simple structures; it cannot analyse structures containing volumetric defects or cases where more than two flaws exist (e.g. crack networks). It is also restricted to cracks which can be characterised as being either elliptical (for embedded flaws) or semi-elliptical (for surface flaws), which is the characterisation convention used in R6 [3] and BS 7910 [2]. Since current fracture assessment procedures use relatively simple interaction rules, int_defects is a useful aid to procedure development despite these limitations. int_defects can also generate finite element models of single semi-elliptical surface defects and elliptical embedded defects. Therefore, in addition to its primary use for investigating defect interaction, int_defects can also be used for parametric studies of single cracks. This is useful for compiling compendia of pre-calculated SIF, limit load and strain energy release rate solutions for use in assessment.

int_defects is distributed as a MATLAB toolbox. It requires installations of the numerical computing environment MATLAB [24], the FE pre-processor Abaqus/CAE [4] and the FE solver Abaqus/Standard [25]. The MATLAB Parallel Computing Toolbox [29] is recommended for processing large sets of models, but is not required. The distribution includes a user guide, a set of examples and commented MATLAB code. Validation of int_defects by comparison of results with well-known elastic, elastic-plastic and limit load solutions has been performed; some example validation cases are given in Appendix A.

2.2. Workflow

Fig. 1 shows the workflow used internally by int_defects. To analyse a set of models of flawed plates or pipes, a user performs the following steps in the MATLAB environment:

1. Decide on the set of cases to be analysed then define a data structure containing parameters which describe these cases. Save the data structure in a MATLAB .mat file.
2. Create and execute the set of models which represent the cases defined in Step 1 using the functions int_defects_write_input_parametric and int_defects_run_parametric_parallel, respectively.
3. Extract the results. Depending on the type of analysis performed, these may be either contour integrals (K, J or elastic T-stress) or limit loads.

Additional actions subsequent to Step 3 will depend on the type of analysis being performed. For example, if the objective of the analysis is to determine elastic interaction factors (see Eq. (1)) for closely-spaced flaws then Steps 1–3 would be performed twice: once for a set of models of single flaws and once for models of interacting flaws. Then, the interaction factors would be calculated

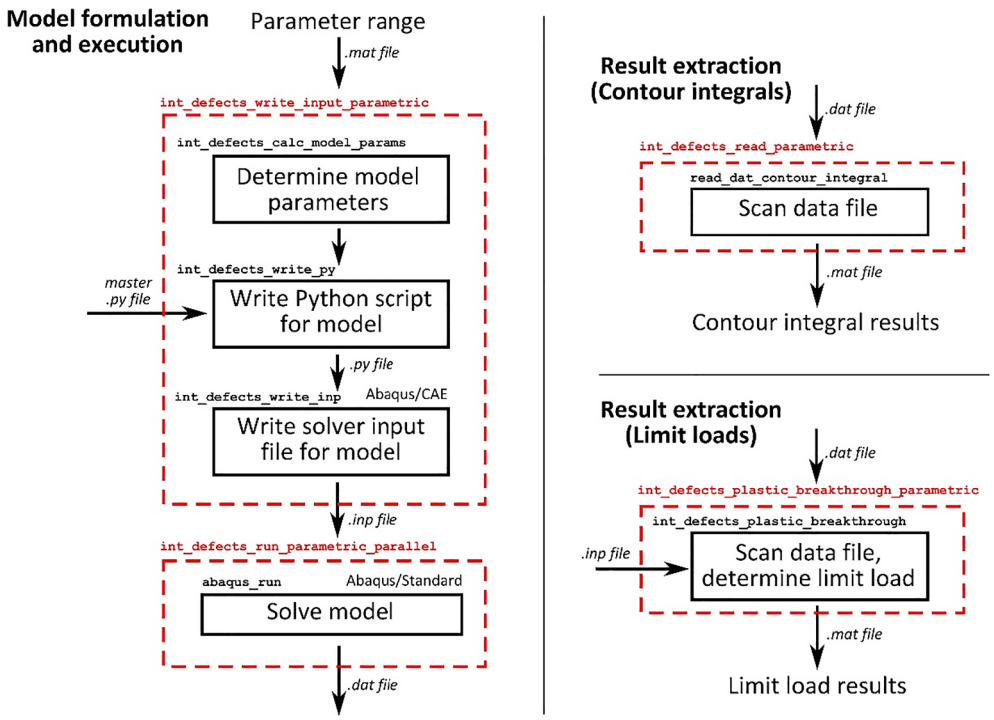

Fig. 1. Workflow elements used by the int_defects toolbox. Red boxes denote key high-level functions which loop over all models in a set. A set of models is formulated and solved (left-hand section), then the results are extracted and post-processed (right-hand sections). Determination of crack tip contour integrals and determination of limit loads require different post-processing methods. (For interpretation of the references to colour in this figure legend, the reader is referred to the web version of this article.)

from the contour integral results (int_defects includes the function int_defects_calc_interaction_factor for this purpose).

3. Usage examples

The following examples illustrate how int_defects can be used and the range of problems that it can solve. Each problem is posed in the form of a question that int_defects is used to answer. Details of the computer hardware used and execution times for each set of models are given in Appendix B.

3.1. Usage example: Elastic interaction between twin surface flaws

Question: "*A large cylindrical pressure vessel contains a two identical crack-like surface flaws in the axial-radial plane. It may be pressurised and/or subjected to thermal shock. To what degree will the flaws interact, according to linear-elastic fracture mechanics theory?*"

The elastic interaction between flaws, i.e. the amount by which the presence of one flaw affects the SIF at another if the material is assumed to be linear-elastic (see Equation 1), is a key factor in judging the significance of flaw interaction for structural integrity. The pressure vessel in this example has a thickness (b) of 166 mm and an internal radius $r_i \gg b$, such that the region containing flaws can be closely approximated by a flat plate in tension. The vessel wall contains a pair of identical internal surface flaws each with a depth (a) of 40 mm, both in the axial-radial plane. The aspect ratio of the flaws ($\frac{a}{c}$) and the inter-flaw spacing (d) are undefined: multiple models with different aspect ratios in the range $\frac{1}{4} \leq \frac{a}{c} \leq 4$ and spacings in the range $8 \text{ mm} \leq d \leq 32 \text{ mm}$ have been used to investigate the effect of these geometric parameters (see Fig. 2). The vessel may be subjected to internal pressurisation, a thermal shock involving a rapid internal quench or a combination of the two. The through-thickness stress profile resulting from the thermal shock is shown in Fig. 3: this approximates the thermal shock load imposed on a nuclear Reactor Pressure Vessel (RPV) experiencing a Medium Loss-Of-Coolant Accident (MLOCA) and internally quenched by emergency coolant injection [30]. Using the assumption that $r_i \gg b$, pressurisation is simulated by a uniform through-wall tension.

70 linear elastic FE models were used to determine the crack tip SIFs occurring in crack pairs with different combinations of aspect ratio, inter-flaw spacing and loading state. 14 models of single cracks with different combinations of aspect ratio and loading state were also performed. Results from these two sets of models were used to determine the elastic interaction factor γ (see Equation 1) as a function of position on the crack tip line. A special-purpose function for calculating elastic interaction factors (int_defects_calc_interaction_factor) is included in the int_defects toolbox. Some of these results, for cracks with an aspect ratio of $\frac{a}{c} = 1$ only, are shown in Fig. 4. For this geometry, the SIF is at a maximum close to the intersection between the crack tip line and the plate surface for both uniform stress and thermal shock loading modes (see Fig. 4a & c). Therefore, assuming a brittle fracture mechanism and ignoring crack-tip constraint effects, fracture would be expected to initiate at this location if the load was sufficient. For both

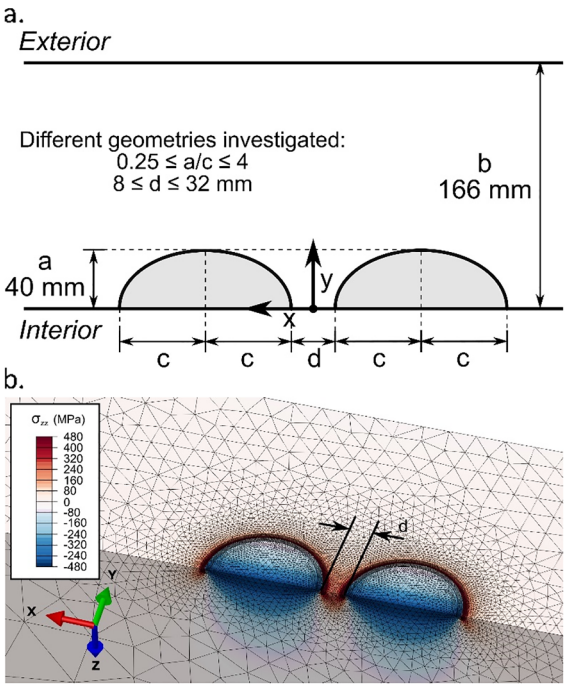

Fig. 2. Model geometry used for investigating the interaction between a pair of identical surface flaws. (a.) Flaw geometry with dimensions in mm. (b.) Close-up of an Abaqus FE model generated using int_defects, with the calculated stress field (crack-normal component shown) resulting from crack-face loads used to represent the thermal shock loading state shown in Fig. 3.

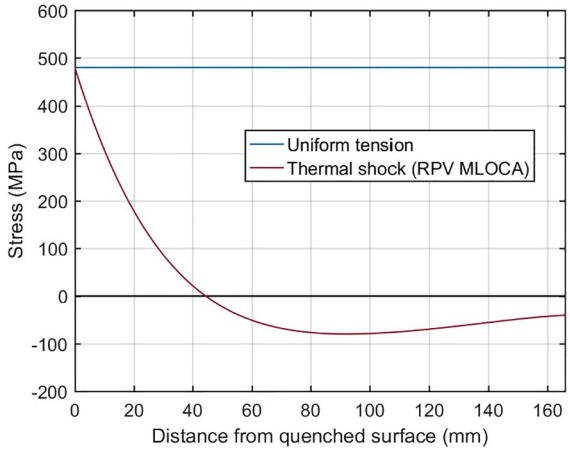

Fig. 3. Through-wall distributions of stress resulting from uniform tension and thermal shock. The thermal shock stress profile was predicted via elastic analysis by González-Albuixech et al. [30] for a RPV 399 s into a MLOCA event. The stress at the internal surface is 480 MPa for both cases.

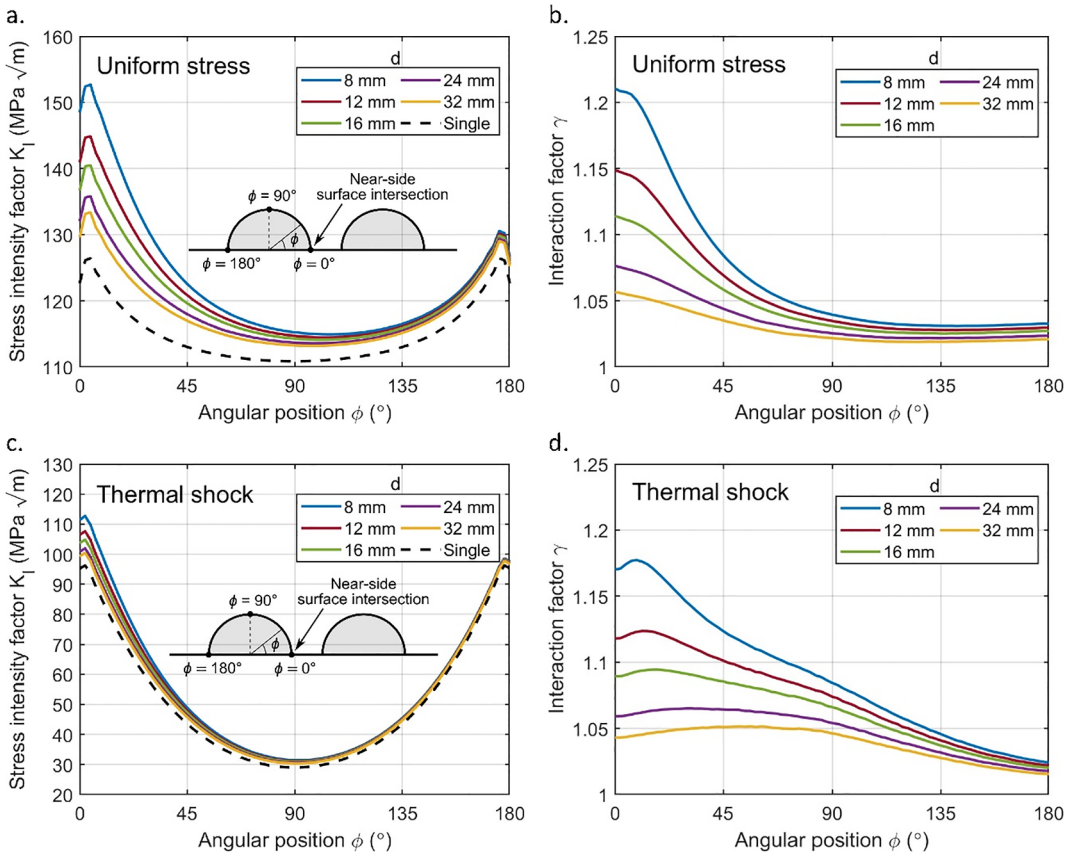

Fig. 4. SIF and elastic interaction factor as a function of position on the crack tip line for pairs of twin semi-circular cracks ($\frac{a}{c} = 1$) separated by different distances d and subjected to the two through-thickness loading conditions shown in Fig. 2. (a.) SIF for cracks subject to a uniform tensile stress and (b.) corresponding interaction factors. (c.) SIF for cracks subject to a thermal shock stress profile and (d.) corresponding interaction factors.

loading cases the SIF distribution which occurs for a pair of flaws is greater than for a single flaw. The SIF increases with decreasing inter-flaw spacing. Despite large differences in the SIF caused by each loading case (Fig. 4a & c), the proportional increase in SIF due to flaw proximity is similar (Fig. 4b & d) but not identical.

Fig. 5 shows the elastic interaction factor at a location close to the near-side surface intersection ($\phi \cong 0^{\circ}$) for pairs of identical cracks with various crack aspect ratios and spacings. Pairs of closely-spaced and wide (i.e. low aspect ratio) flaws under uniform

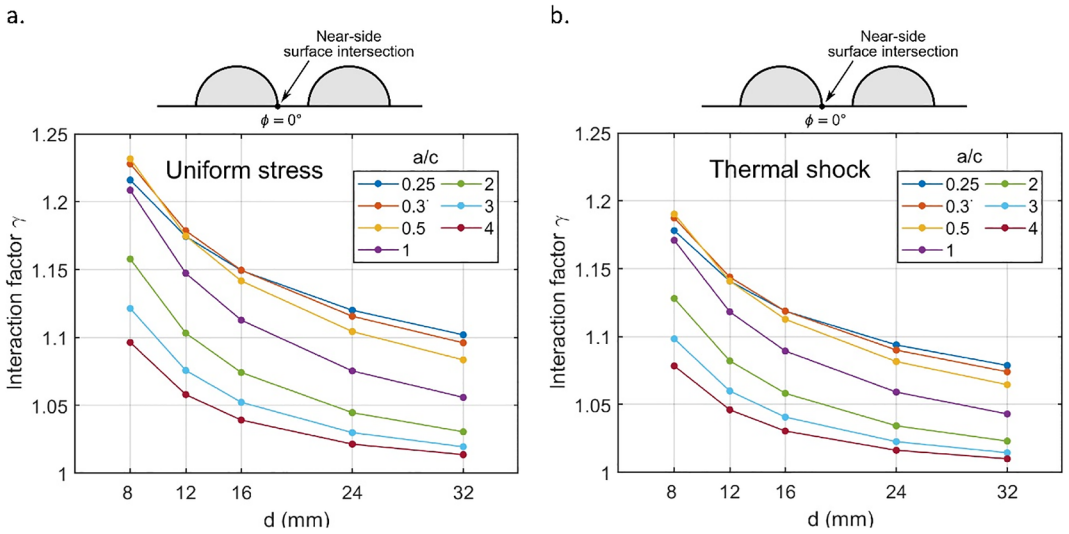

Fig. 5. Stress intensity interaction factor for the near-side surface point ($\phi \cong 0^{\circ}$) in twin surface crack pairs subjected to the through-wall loading cases shown in Fig. 3. (a.) uniform stress and (b.) thermal shock.

stress interact most strongly. This interaction causes a maximum increase in near-side SIF of 20–25% with respect to a single crack for the closest, widest geometries considered (Fig. 5a). If necessary, FE results for the two loading cases could be linearly superimposed to determine the elastic interaction factors under combined pressurisation and thermal shock.

3.2. Usage example: Determination of single-flaw limit loads

Question: "*What are the local and global plastic limit pressures for thick-walled pipes with an inner to outer radius ratio of 0.8, and containing single axial surface flaws of known size and shape? Are existing formulae for determining the limit pressures of axially flawed pipes accurate?*"

Plastic limit pressures are a key input in many structural integrity assessment procedures. In this example, int_defects was used to determine the limit pressures of thick-walled pipes containing surface-breaking axial flaws on the internal or external surface, for a wide range of flaw depths and aspect ratios. The analysis was used to determine the local limit pressure p_{LL} (i.e. the pressure at which a plastic ligament forms connecting the flaw and the opposite wall of the pipe) and the global limit pressure p_{GL} (i.e. the pressure at

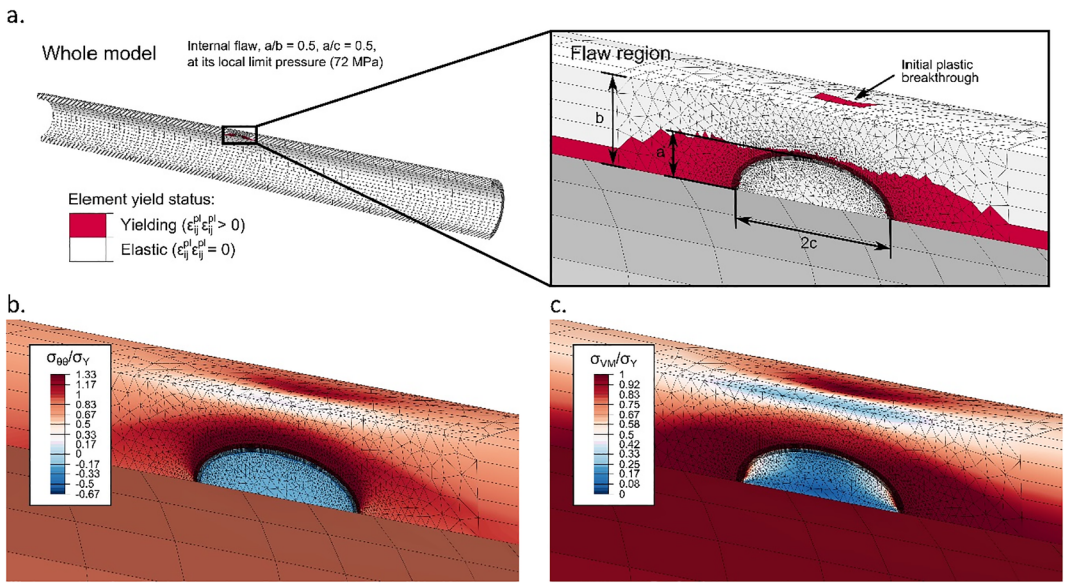

Fig. 6. Elastic → perfect-plastic model of a pipe containing an internal surface flaw in the axial-radial plane at the local limit pressure. The flaw dimensions are $\frac{a}{b} = 0.5$ and $\frac{a}{c} = 0.5$ in this example. (a.) Element-wise plastic yielding status – note breakthrough of the yielding zone to the pipe's exterior surface. (b.) Circumferential stress component. (c.) von Mises stress – note $\sigma_{VM} \leq \sigma_Y$.

which global plastic instability occurs). The pipe geometry is shown in Figs. 6 and 7: the pipe has a ratio of inner to outer radius of 0.8. A parametric set of 77 FE analyses was performed to determine the limit loads for pipes containing crack-like flaws with normalised depths ($\frac{a}{b}$) in the range $\frac{1}{8} < \frac{a}{b} < \frac{7}{8}$ and aspect ratios ($\frac{a}{c}$) in the range $\frac{1}{8} < \frac{a}{c} < 4$. The pipe material was modelled as being elastic-plastic with a von Mises yield locus and no strain-hardening. The elastic properties were taken as E = 210 GPa and $\nu = 0.3$ and the (arbitrary) elastic limit stress, or yield stress, is denoted σ_Y. A monotonically-increasing pressure was applied to the pipe's internal surface and any internal crack faces.

An example of a model created by int_defects is shown in Fig. 6. The local limit pressures were determined using a function for this purpose included in the int_defects toolbox (int_defects_plastic_breakthrough). Pressurisation to the global limit causes plastic instability, so the global limit pressure was determined from the last completed model increment. Plastic limit pressures for internally and externally cracked pipes are shown in Fig. 7. As expected, the limit pressures are lowest for pipes containing deep, wide cracks. For very shallow and narrow cracks, the results converge towards the theoretical limit pressure for an unflawed thick-walled pipe p_{UL} [31–33]:

$$p_{UL} = \frac{2}{\sqrt{3}}\sigma_Y \ln\frac{r_o}{r_i} \tag{2}$$

where r_i and r_o are the pipe inner and outer radii respectively, and σ_Y is the material's elastic limit stress (which is equivalent to the yield stress for a non-strain-hardening material). The results in Fig. 7a and c were compared with the (semi-analytical) formulae for flawed pipe local limit pressures given by Lei [33] and included in Annex P of BS 7910:2013 [2]. The BS 7910 formulae are calculated assuming a rectangular rather than semi-elliptical surface flaw profile and are given in Appendix C. Fig. 8 shows that the formula for external flaws gives a slightly lower local limit pressure than calculated via FEA for all cases, i.e. a slightly conservative estimate. On the other hand, the formula for external flaws predicts a higher local limit pressure than indicated by FEA for some cases: mainly for relatively deep cracks ($\frac{a}{b} > 0.375$). This result supports the continued use of the formula for internal flaw local limit pressure but suggests that the formula for external flaws could be reviewed.

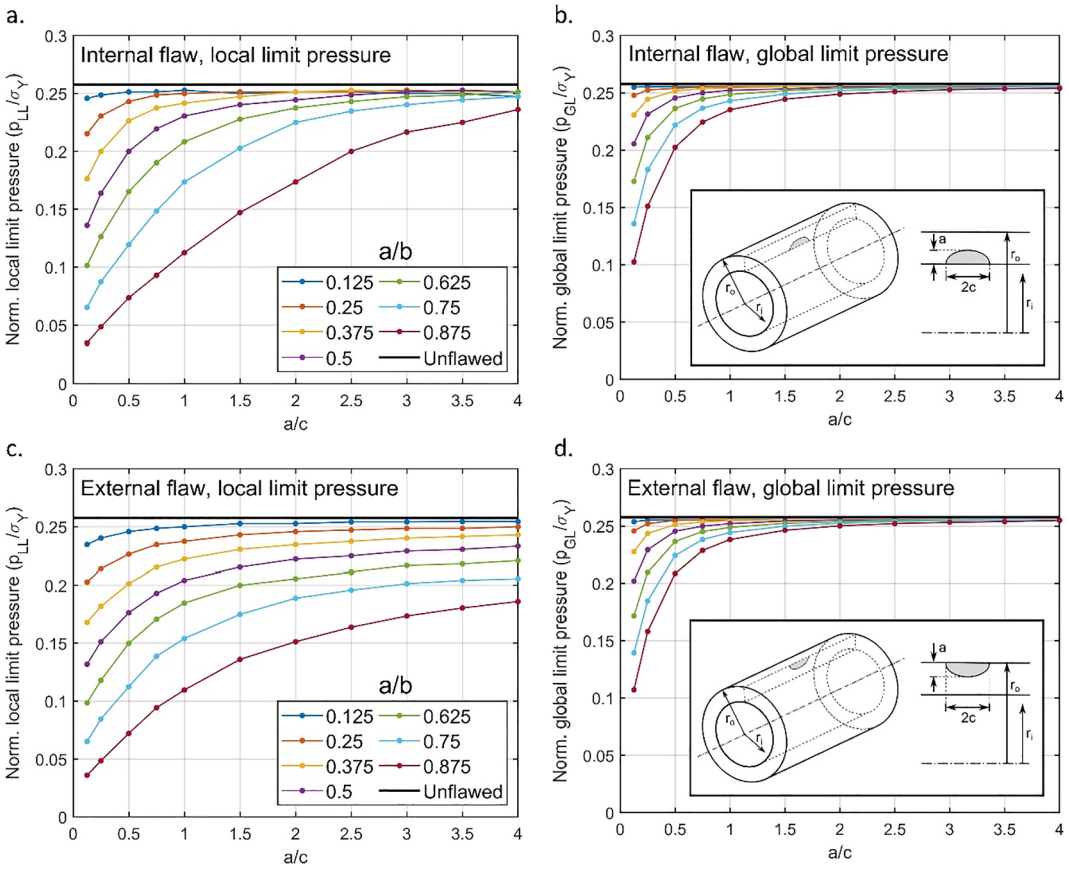

Fig. 7. Limit pressures for thick-walled, closed-ended pipes with $\frac{r_i}{r_o} = 0.8$ containing axially-aligned surface flaws, determined via FEA. A von Mises yield locus with no strain-hardening is assumed. (a.) local limit for internal flaws, (b.) global limit for internal flaws, (c.) local limit for external flaws, (d.) global limit for external flaws.

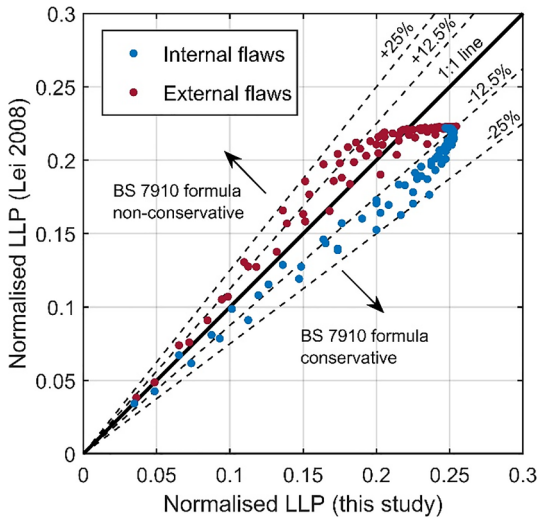

Fig. 8. Accuracy of formulae used in Annex P of BS 7910:2013 for estimating the local limit pressure for pipes with surface-breaking axial cracks [2,33]. Local limit pressures for 154 cases are shown, normalised using $\frac{P_{LL}}{\sigma_Y}$. For some external cracks, the current BS 7910:2013 formula produces a potentially non-conservative result.

3.3. Usage example: J-integral analysis for interacting flaws

Question: "*A surface flaw and an embedded flaw occur close to one another in a wide steel plate under tension. How does the depth of the embedded flaw affect the load and crack tip location at which fracture will initiate?*"

The steel plate has a thickness (b) of 80 mm and is acted upon by a remotely-applied tensile stress which is increased monotonically from 0 to 500 MPa. The plate contains two crack-like flaws in the same through-thickness plane, shown in Fig. 9. There is a surface-breaking flaw with a depth (a_1) of 20 mm and a total width ($2c_1$) of 40 mm, and an embedded flaw with a total size in the depth direction ($2a_2$) of 20 mm, a total size in the width direction ($2c_2$) of 40 mm, and a depth below the plate's surface denoted by d_2. The material is relatively brittle, with a fracture initiation toughness of $J_{0.2} = 80\,\mathrm{N\,mm^{-1}}$.

The plate material is modelled using incremental plasticity theory and its mechanical response is taken to follow a Ramberg-Osgood relationship [34]:

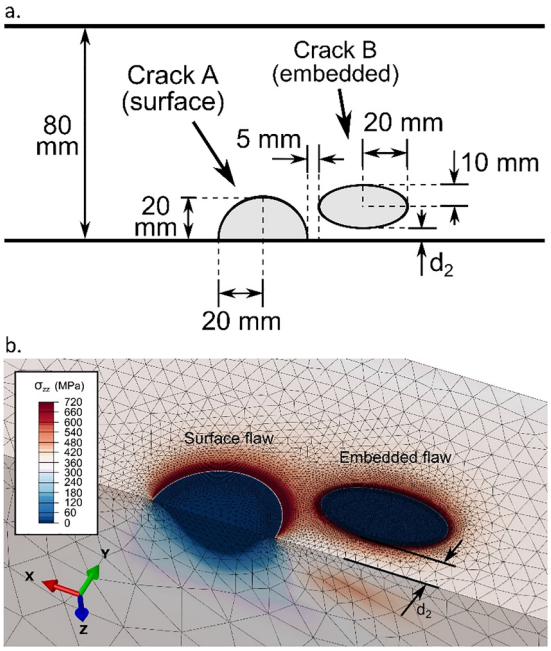

Fig. 9. A pair of interacting coplanar crack-like flaws in a plate - one surface and one embedded. (a.) Flaw geometry. (b.) Close-up of an Abaqus FE model generated using int_defects, with the calculated stress field (crack-normal component shown) for a remotely applied tensile stress of 360 MPa.

$$\varepsilon = \frac{\sigma}{E} + \alpha\frac{\sigma}{E}\left(\frac{\sigma}{\sigma_Y}\right)^{n-1} \tag{3}$$

where the Young's modulus $E = 210$ GPa, yield stress $\sigma_Y = 360$ MPa, yield offset parameter $\alpha = 1.667$ and hardening coefficient $n = 12$. The material is assumed to exhibit a von Mises yield locus and isotropic strain-hardening behaviour. Although a fictional material which follows a Ramberg-Osgood relationship is used in this example, in general int_defects can use any monotonic true stress-strain curve.

int_defects was used to generate and run a set of FE models of this crack pair to investigate the effect of the embedded crack depth (parameter d_2, see Fig. 9) in the range $5 \leq d_2 \leq 20$ mm. The J-integral as a function of position on each crack tip line was extracted from the results; this is shown in Fig. 10 for an applied tensile stress of 360 MPa. Two factors increase the J-integral over part of the crack tip lines of the interacting flaws: the proximity of the embedded flaw to the plate's surface and the proximity of the two flaws to each other. In this configuration, fracture would be expected to initiate from the surface flaw at the point closest to the embedded flaw ($\phi_1 \cong 27^\circ$), which is the location that experiences the greatest J-integral (see Fig. 10). However, if the embedded flaw is located only 5 mm deep then tearing-out of the embedded flaw may occur simultaneously at $\phi_2 \cong 268^\circ$.

4. Discussion and conclusions

The above examples illustrate the range of analyses that can be performed using the int_defects toolbox. The number of individual FE models used in each of these examples is relatively small, but the toolbox is designed for scalability and contains features for ensuring robust execution of large sets of models and for error-checking FE results. Model sets containing thousands of individual FE analyses are feasible [22]. Although int_defects is limited in terms of the geometries that it can analyse, it provides a rapid and scalable way to investigate defect interactions.

Flaw interaction criteria are normally used at the start of fracture-mechanics-based structural integrity assessment procedures. Consequently, they affect the rest of the assessment and often have a decisive impact on the outcome. In most procedures, the criteria for flaw interaction are based on the geometry and spacing of the flaws. Other factors such as a loading state and material ductility are rarely taken into account, although a few procedures (such as SINTAP [35]) do consider these. int_defects can be used to examine different flaw geometries as well as factors such as loading state. It has been used to evaluate flaw interaction and recharacterisation rules in recent studies on the BS 7910 interaction criteria [36], the BS 7910 Annex E buried-to-surface recharacterisation rules [37], and the interaction criteria of various procedures including R6 [22].

In summary, int_defects is a useful tool for studying flaw interactions. It is simple to use, scalable and open-source. Although the range of 3D geometries that it supports is limited, its design instead emphasises features that are useful for formulating interaction criteria and recharacterisation rules, including automatic SIF and limit load analysis, easy parameterisation of the geometry and loading state, and robustness when handling large sets of models.

Data access statement

- The int_defects toolbox (v1.2.0) is available from the University of Bristol data repository: http://data.bris.ac.uk/data/dataset/2s1zavsbkctna2bnh6g6os9n2k
- The underlying data for all examples shown in this paper can be downloaded from: http://data.bris.ac.uk/data/dataset/36wlnpm16muu52ppxhzaa0udz2

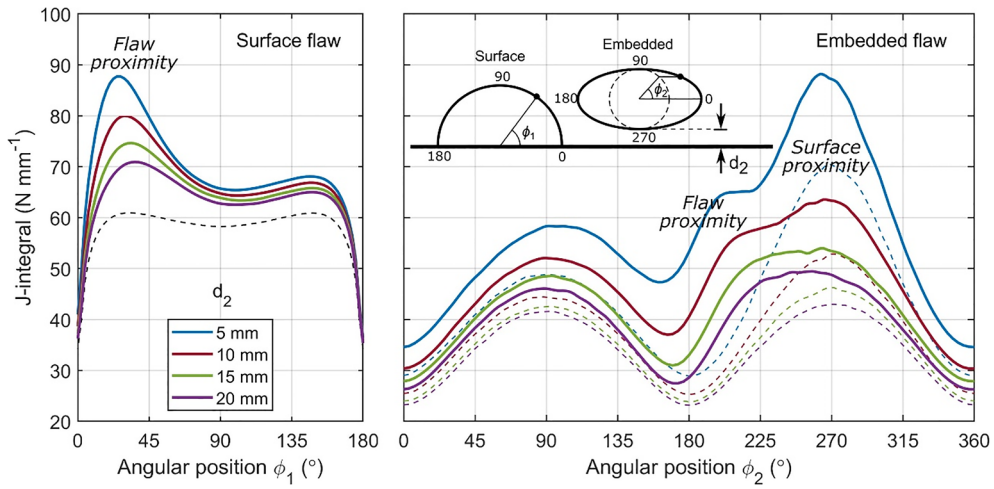

Fig. 10. J-integral as a function of position on each flaw in the interacting pair shown in Fig. 9, at an applied remote stress of 360 MPa (i.e. σ_Y). Results for three different embedded flaw depths are shown. Dashed lines show the J-integral for each flaw in isolation.

Declaration of Competing Interest

The authors declare that they have no known competing financial interests or personal relationships that could have appeared to influence the work reported in this paper.

Acknowledgements

The authors are grateful to Dr Bostjan Bezensek for many discussions on the background to this work. The work was funded by the UK Engineering and Physical Sciences Research Council (EPSRC) under grant no. EP/M019446/1, and by the EPSRC impact acceleration account EP/R511663/1.

Appendix A. Validation

Validation studies have been performed to check the accuracy of results from int_defects against well-known existing solutions and three validation cases are presented here. The toolbox can be applied to a wide range of situations so we recommend that users also perform their own validation studies specific to their particular application. Note that:

- int_defects can perform several different types of analysis: calculation of elastic or elastic-plastic crack tip field parameters and calculation of local or global limit loads. These different types of analysis should each be validated individually because they have different potential sources of error.
- int_defects allows the user to change model parameters that can affect the accuracy of the result, such as the model's time incrementation and crack tip mesh density. However, the toolbox is designed so that leaving these parameters to take default values will generally produce accurate results.
- Different applications of int_defects may require different levels of accuracy.
- Typically, int_defects is used to determine results for a wide range of crack geometries, component geometries and/or loading conditions. In most cases, pre-existing results for comparison will only exist for certain combinations of geometry/loading.

In addition to the examples shown below, comparisons of results from int_defects with the results of other authors are presented by Coules [22] (elastic analysis of twin surface cracks) and Coules & Bezensek [38] (limit load analysis of single surface cracks).

A.1. Validation case: Elastic analysis of single surface cracks

This example aims to validate int_defects' capability for elastic cracked-body analysis. Stress intensity factors for single semi-elliptical surface cracks in wide elastic plates of finite thickness were determined and compared with the well-known numerical results of Newman & Raju [39], as well as a wide range of results for this geometry from different sources.

Newman & Raju investigated cracks in the plane normal to the loading direction, with normalised depths in the range $0.2 \leq \frac{a}{b} \leq 0.8$ and aspect ratios in the range $0.2 \leq \frac{a}{c} \leq 2$. The plate material was defined to have a Poisson's ratio $\nu = 0.3$ and an arbitrary elastic modulus was used (since this does not affect the stress intensity factor result). Two loading cases were investigated: pure tension resulting in a crack-transverse stress of unit magnitude, and pure bending resulting in a stress of unit magnitude at the plate's surface. A typical stress field for such cases determined using int_defects is shown in Fig. 11.

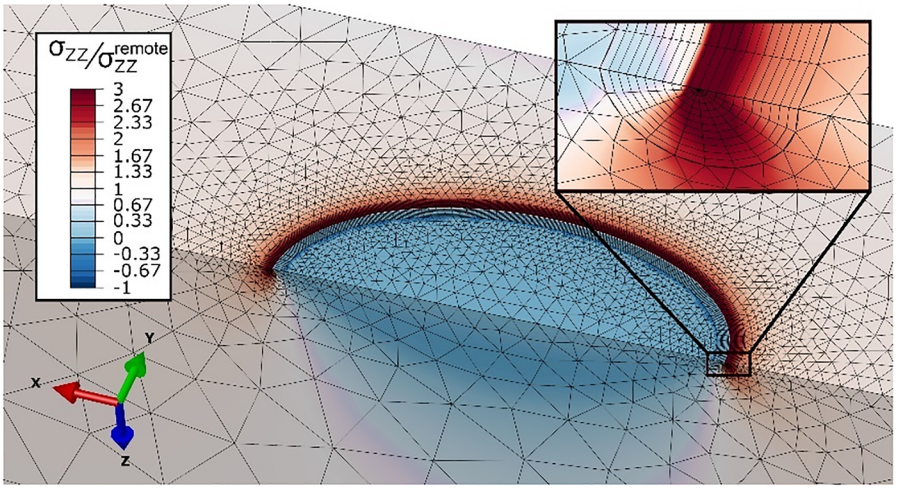

Fig. 11. Typical mesh used for linear elastic analysis of a semi-elliptical surface crack in this validation case. The result for a crack with dimensions $\frac{a}{c} = 0.6$ and $\frac{a}{b} = 0.4$ under remote tension is shown.

A comparison of results is shown in Fig. 12 (tension) and Fig. 13 (bending). The results are given in normalised form as $\frac{K_I}{\sqrt{\pi a / Q}}$ where Q is a shape factor for elliptical cracks which is approximated by [39,40]:

$$Q \cong 1 + 1.464\left(\frac{a}{c}\right)^{1.65} \quad for \quad \frac{a}{c} \leq 1 \tag{4a}$$

$$Q \cong 1 + 1.464\left(\frac{c}{a}\right)^{1.65} \quad for \quad \frac{a}{c} > 1 \tag{4b}$$

For both the tension and bending cases, there is good agreement between the results of int_defects and those of Newman & Raju. The largest discrepancies occur for very wide cracks ($\frac{a}{c} = 0.2$) and are believed to be due to the low level of mesh refinement used by the earlier authors. In the bending case, some more recent results by Lei [41] are also presented - these also show good agreement

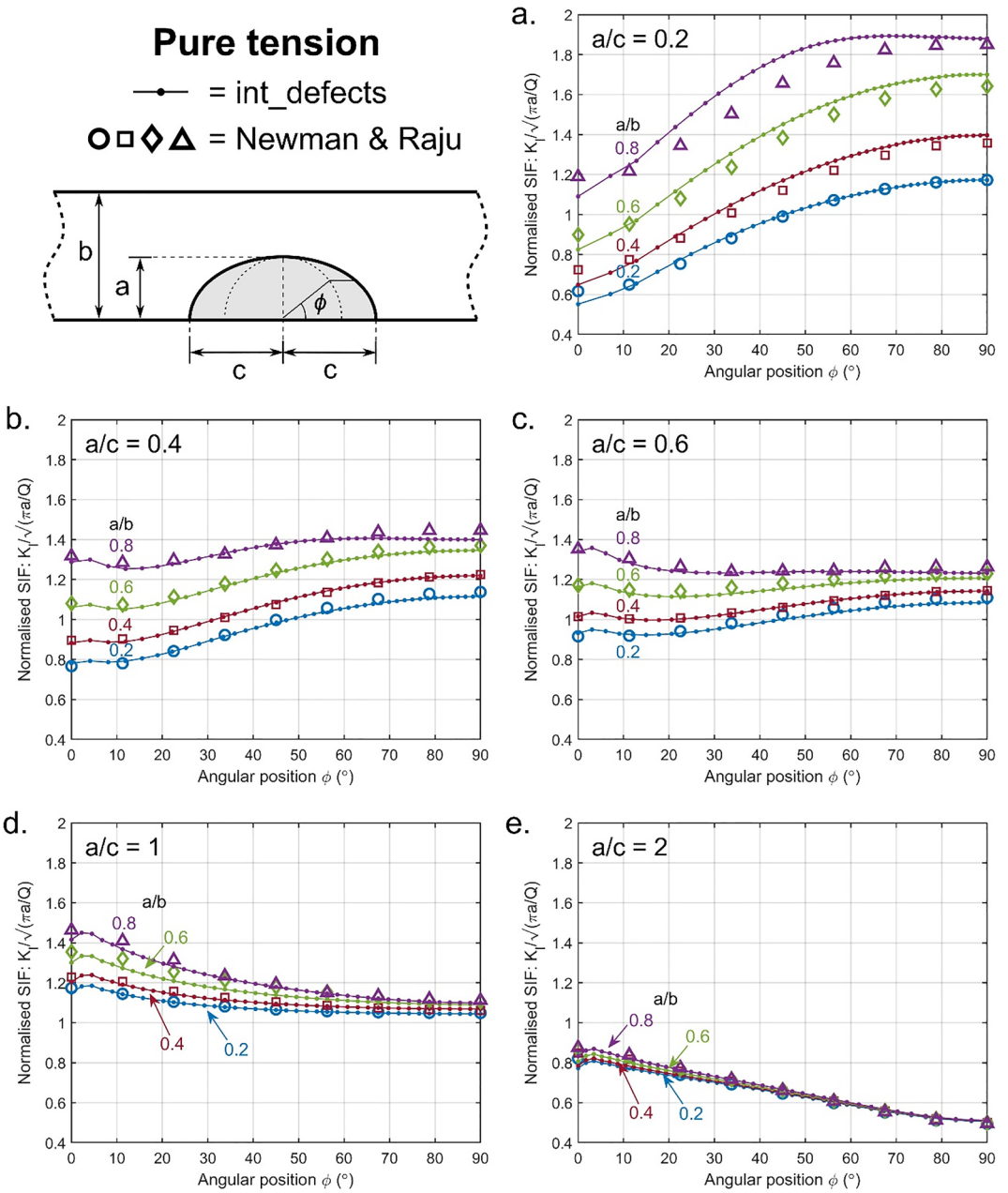

Fig. 12. Normalised stress intensity factor as a function of position on the crack tip line for 20 semi-elliptical surface cracks with different depths (a/b) and aspect ratios (a/c) in wide plates subjected to a unit tensile stress. Good agreement is observed between the results of int_defects and Newman & Raju [39].

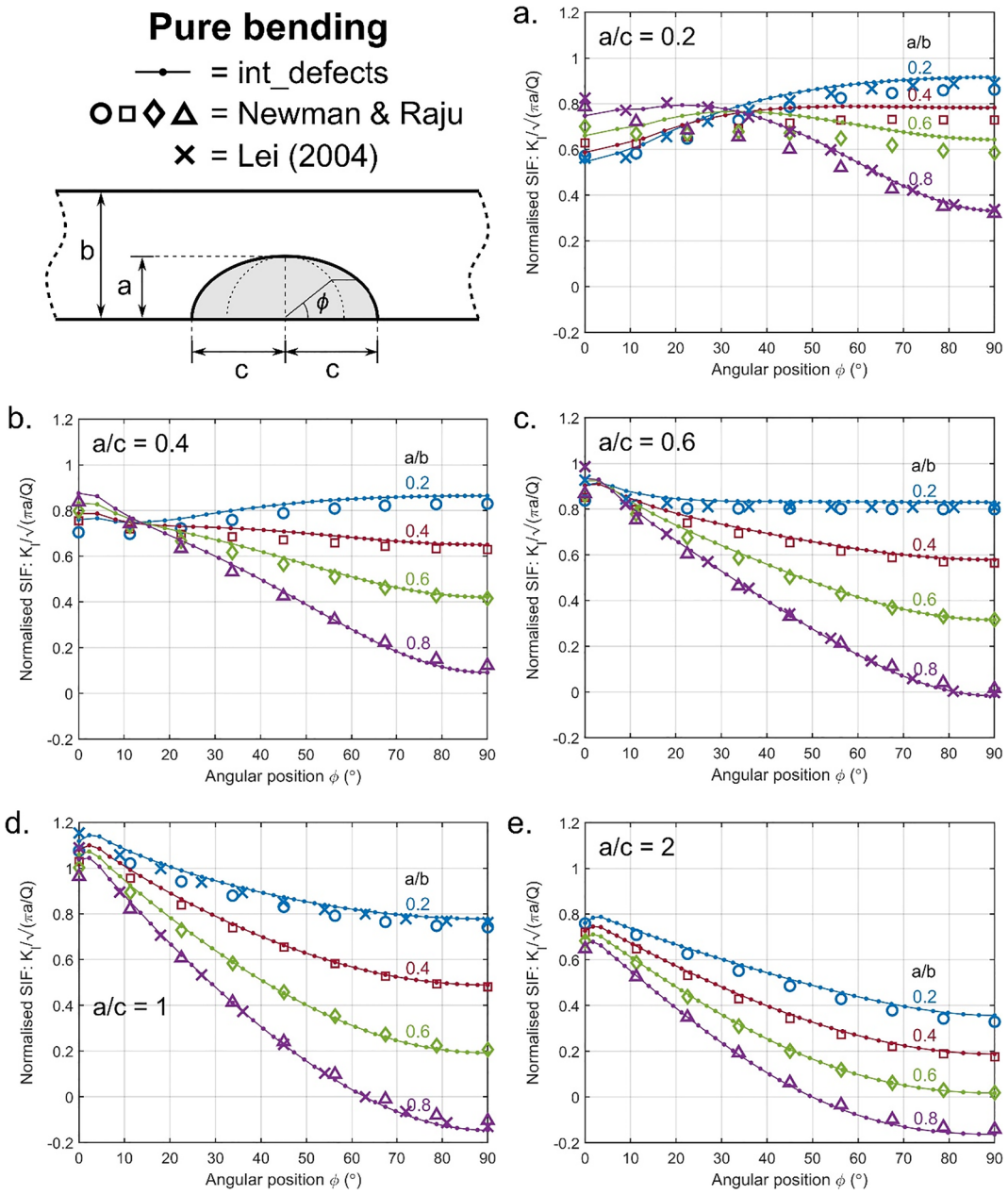

Fig. 13. Normalised stress intensity factor as a function of position on the crack tip line for 20 semi-elliptical surface cracks with different depths (a/b) and aspect ratios (a/c) in wide plates subjected to a pure bending, causing unit stress at the plate's surface. Good agreement is observed between int_defects results and those of Newman & Raju [39] and Lei [41].

with int_defects.

A set of similar models was used to determine the SIF for surface cracks with an aspect ratio of $\frac{a}{c} = 0.6$ and normalised depths in the range $0.05 \leq \frac{a}{b} \leq 0.9$ loaded in remote tension. The SIF at the deepest point in each crack was compared with results from a variety of other authors, as shown in Fig. 14. The int_defects result agrees well with those from other sources, lying close to where the highest density of results is seen.

A.2. Validation case: Limit loads of plates containing offset embedded cracks

In this example, global limit loads for finite plates containing embedded offset elliptical cracks are determined using int_defects and compared with results of FEA by Li et al. [51]. The geometry is shown in Fig. 15: a flat plate is loaded in tension normal to the crack plane. The global limit loads for plates of this type were determined for all combinations of the following geometric parameters:

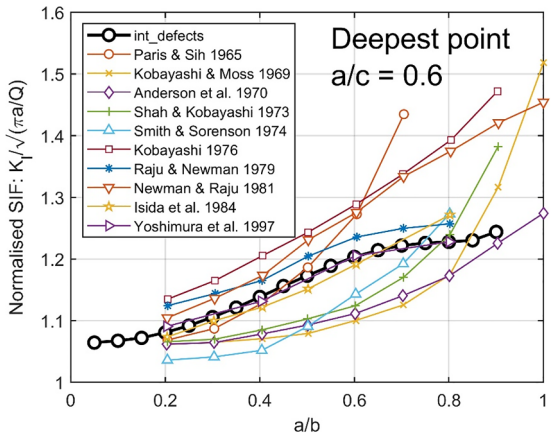

Fig. 14. Comparison of SIF results for semi-elliptical surface cracks in a plate under tension from different authors [18,42–50]. Normalised SIF at the deepest point in cracks with different depths and a constant aspect ratio of a/c = 0.6 is shown. After Isida et al. [42] and Yoshimura et al. [18].

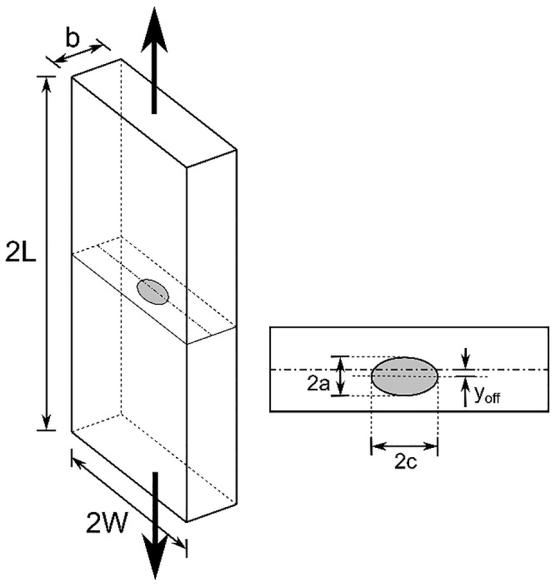

Fig. 15. Flat plate in tension with an embedded semi-elliptical crack offset from the mid-thickness.

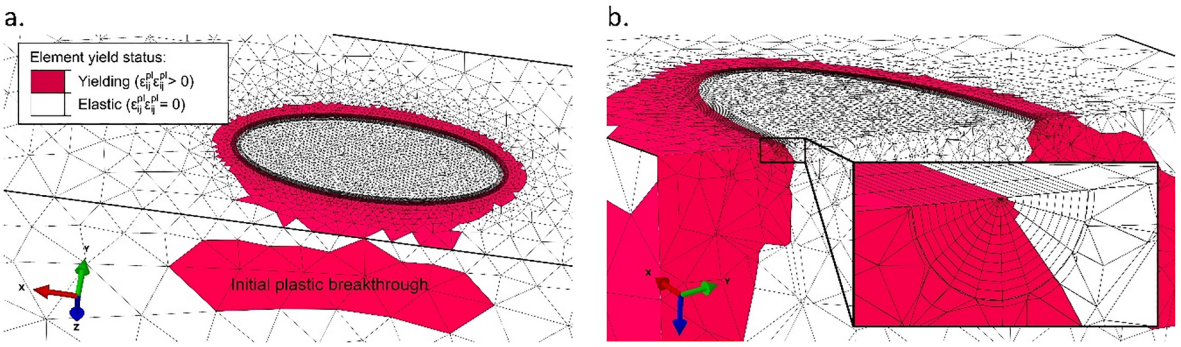

Fig. 16. Finite element model of a plate containing an offset elliptical crack under tension, generated using int_defects to determine plastic limit loads. The case shown has the geometric parameters $\frac{c}{W} = 0.3$, $\frac{a}{c} = 0.4$, $\frac{a}{b} = 0.2$, $\frac{y_{off}}{b} = 0.2$. The element-wise plastic yielding status is shown at the local limit load (320 MPa remote tension). a. Overview of the cracked region, b. cross-section of the cracked region showing the crack tip mesh.

normalised crack depth $\frac{a}{b} = 0.1, 0.2, 0.3$, crack aspect ratio $\frac{a}{c} = 0.2, 0.4, 1$ and offset parameter $\frac{y_{off}}{b} = 0, 0.2, 0.4$. For the cases investigated by Li et al., the overall plate width (W) was linked with the crack width (c), i.e.:

$$\frac{c}{W} = 0.4 \quad when \quad \frac{a}{c} = 0.2 \tag{5a}$$

$$\frac{c}{W} = 0.3 \quad when \quad \frac{a}{c} = 0.4 \tag{5b}$$

$$\frac{c}{W} = 0.2 \quad when \quad \frac{a}{c} = 1 \tag{5c}$$

int_defects was used to create and solve elastic → perfectly-plastic models for all combinations of $\frac{a}{b}$, $\frac{a}{c}$ and $\frac{y_{off}}{b}$ above. The material was defined as exhibiting incremental flow plasticity with a von Mises yield locus and no strain-hardening. The limit stress (σ_Y) had a nominal value of 360 MPa, and elastic parameters $E = 210$ GPa and $\nu = 0.3$ were used. Large-displacement (i.e. geometrically non-linear) spatial modelling was used for the analysis. An example of the finite element mesh used is shown in Fig. 16.

Fig. 17 shows a comparison of global limit loads for this geometry (n_{GL}) determined using int_defects with FEA results from Li et al. [51]. Good agreement is observed between the two sets of limit load predictions across the full range of geometric parameters: the global limit loads determined using int_defects differ from the results of Li et al. by a maximum of 3%. int_defects consistently predicts a slightly higher global limit load, which is probably due to differences in the modelling methods used. For example, int_defects determines the global limit load from the point at which the FEA solver is unable to continue due to global plastic instability whereas Li et al. determined the global limit load from the plate's load-displacement curve. The analysis with int_defects also used geometrically non-linear analysis, whereas Li et al. used a small-displacement formulation. Nevertheless, close agreement between the two sets of results demonstrates the accuracy of int_defects for limit load analysis.

A.3. Validation case: ASTM analytical round robin for elastic-plastic analysis

This example is based on an ASTM inter-laboratory round robin study concerning elastic-plastic analysis of a surface-cracked plate under tension, full details of which are reported by Wells & Allen [52]. The single specimen used in Phase 1 of the study was a flat plate of 2219-T8 aluminium alloy containing a semi-elliptical surface crack in the plane normal to the loading direction. The plate was subjected to a monotonically-increasing tensile load. Experienced participants from 15 institutes were invited to predict the J-

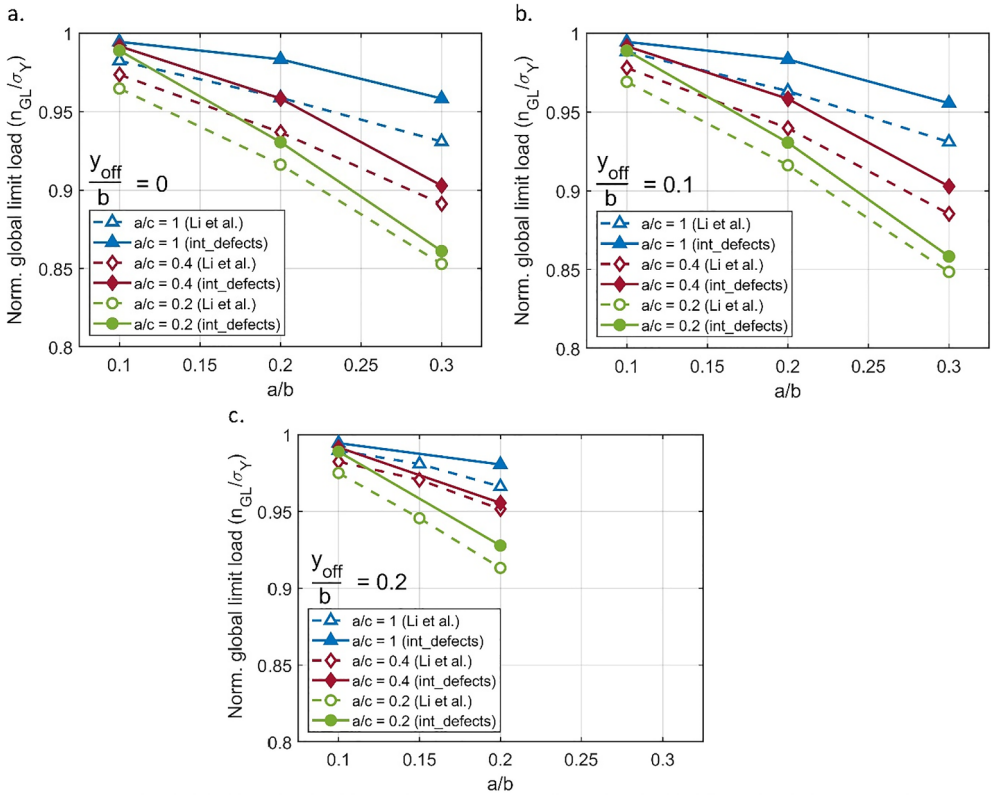

Fig. 17. Normalised global limit loads of finite plates containing elliptical embedded flaws, loaded in tension (as shown in Fig. 15). Results for plates with different crack depths ($\frac{a}{b}$), aspect ratios ($\frac{a}{c}$) and through-thickness offset parameters ($\frac{y_{off}}{b}$) are given. (a.) $\frac{y_{off}}{b} = 0$, (b.) $\frac{y_{off}}{b} = 0.1$, (c.) $\frac{y_{off}}{b} = 0.2$.

integral as a function of load and position on the crack tip line using numerical modelling. The study was performed 'blind': participants were told the specimen's geometry, its loading conditions and material tensile test data, but not to the results of other participants.

A model of an equivalent surface-cracked plate under tension was created automatically using int_defects; the mesh is shown in Fig. 18. Elastic-plastic mechanical properties were defined using the same material uniaxial tensile test data that were provided to the study participants. The analysis performed with int_defects assumed that the material exhibited incremental plastic flow with a von Mises yield locus and isotropic strain-hardening behaviour. A comparison of results from int_defects with the results of the 15 participants is shown in Fig. 19. The int_defects result lies close to where the highest density of results from round robin participants is observed. This demonstrates that int_defects is able to determine the elastic-plastic crack driving force with equivalent precision to that of a purpose-built finite element model from an experienced analyst.

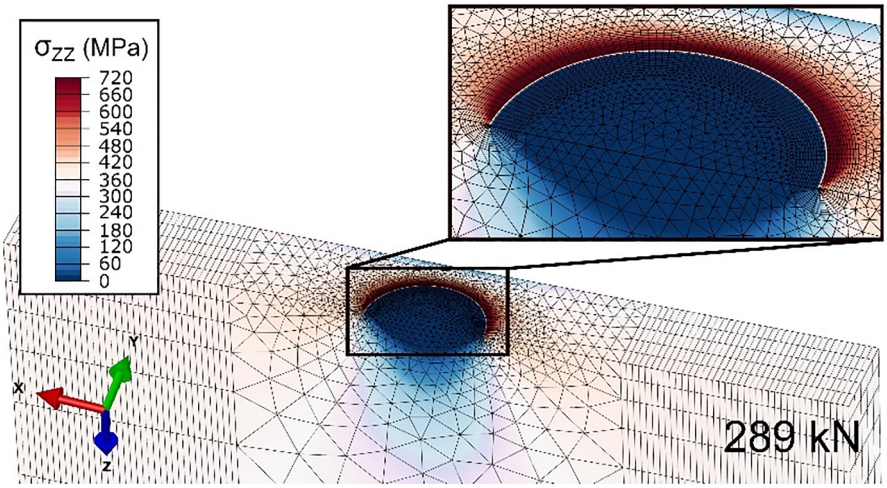

Fig. 18. Automatically generated mesh used for inelastic analysis of a surface crack in a 2219-T8 aluminium alloy plate under tension. The stress field at the maximum tenile load of 289 kN is shown.

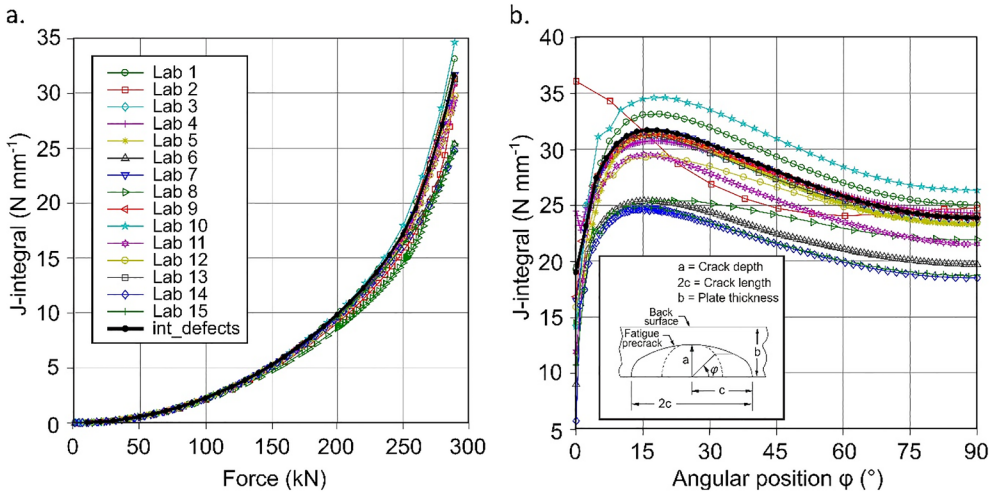

Fig. 19. Contour integral results from elastic-plastic analysis of a surface-cracked plate under tension, comparing int_defects with 15 participants from an ASTM analytical round-robin study [52]. (a.) J-integral at $\varphi = 17^{\circ}$ as a function of applied tensile force. (b.) J-integral as a function of crack tip position at an applied force of 289 kN.

Appendix B. Computing resources and execution times

All analyses discussed in this article were performed using a server machine with 12 Intel Xeon x5670 CPUs and 50 GB of RAM running CentOS Linux 6.8. The software versions used were MATLAB R2017a, int_defects v1.2.0, Abaqus/CAE v6.12 and Abaqus/Standard v6.12. Table 1 lists the average times taken to pre-process (i.e. generate a solver input file) and execute a single finite

Table 1
Average pre-processing and execution times per finite element model for all analyses discussed in this article, and the total time taken to process each model set. All times are given as the elapsed real time ("wall-clock" time).

Article section	Description of model set	Models in set	Mean pre-processing time (s)	Mean execution time (s)	Parallel solver instances	CPUs per solver instance	Total time (hr)
3.1	Elastic interaction (interacting surface cracks)	70	36	415	1	4	7.2
3.1	Elastic interaction (single surface cracks)	14	20	46	1	2	0.3
3.2	Cracked pipe limit loads	154	39	4977	2	4	109.3
3.3	J-integral analysis for interacting cracks (interacting cracks)	4	62	17,747	2	2	11.1
3.3	J-integral analysis for interacting cracks (single surface cracks)	1	21	2118	1	4	0.6
3.3	J-integral analysis for interacting cracks (single embedded cracks)	4	41	7760	2	2	4.7
A.1	Elastic analysis of single surface cracks	40	45	80	2	4	1.0
A.2	Limit loads for plates with offset embedded cracks	24	73	3415	1	4	23.4
A.3	ASTM analytical round robin for elastic-plastic analysis	1	31	662	1	4	0.2

element model for each of the examples presented in this article. For some sets of models, int_defects was used to execute models in parallel by employing multiple instances of the FE solver. This secondary parallelisation can significantly reduce the total time necessary to process the model set. Therefore, Table 1 also gives the total processing time for each set of models, for which the following relationship holds:

$$Total\ time \cong\ No.\ \ models \times \left(Mean\ pre - -processing\ time + \frac{Mean\ execution\ time}{No.\ \ solver\ instances} \right) \tag{6}$$

Appendix C. Existing limit load solutions for axially-flawed pipes

The following approximate solutions for the local limit pressure of thick-walled pipes containing single crack-like surface flaws in the axially-radial plane are given by Lei [33] and used in Annex P of BS 7910:2013 [2]. The geometry is shown in Fig. 7b & d. These formulae assume a von Mises yield locus and a rectangular flaw shape. The solution for flaws on the internal pipe surface includes consideration of the internal pressure acting on the crack faces. Fig. 8 shows a comparison of limit loads determined by these formulae with finite element results from int_defects, for a pipe with a radius ratio $\frac{r_i}{r_o} = 0.8$ and a range of crack dimensions. For internal flaws:

$$\frac{p_{LL}}{\sigma_Y} = \frac{1}{\frac{h_1}{c} + 1}\left[\frac{h_1}{c}\ln(1 + \eta_i) + f_{ps}(1 + \alpha_1\eta_i)\ln\left(\frac{1 + \eta_i}{1 + \alpha_1\eta_i} \right) \right] \tag{7a}$$

where:

$$\frac{h_1}{c} = \frac{(1 - \alpha_1)f_{ps}\left[\ln(1 + \alpha_1\eta_i) - \alpha_1\eta_i\ln\left(\frac{1+\eta_i}{1+\alpha_1\eta_i} \right) \right]}{M_{in}\left\{ \ln(1 + \eta_i) - f_{ps}\left[\frac{1}{M_{in}}\ln(1 + \alpha_1\eta_i) + \left[1 + \alpha_1\eta_i\left(1 - \frac{1}{M_{in}} \right) \right]\ln\left(\frac{1+\eta_i}{1+\alpha_1\eta_i} \right) \right] \right\}} \tag{7b}$$

$$f_{ps} = \frac{1}{1 + \frac{1}{2}\alpha_1\eta_i} \quad for \quad \Phi \le 1 \tag{7c}$$

$$f_{ps} = \frac{\Phi}{\Phi + \frac{1}{2}\alpha_1\eta_i} \quad for \quad \Phi > 1 \tag{7d}$$

and:

$$M_{in} = \left[1 + 1.4\frac{\alpha_1\eta_i}{\Phi^2(1 + \alpha_1\eta_i)} \right]^{\frac{1}{2}} \tag{7e}$$

$$\alpha_1 = \frac{a}{b} \tag{7f}$$

$$\eta_i = \frac{b}{r_i} \tag{7g}$$

$$\Phi = \frac{a}{c} \tag{7h}$$

In these equations, α_1 is the normalised flaw depth, η_i is a wall thickness parameter, and Φ is the aspect ratio. For external flaws:

$$\frac{p_{LL}}{\sigma_Y} = \frac{1}{\frac{h_2}{c} + 1}\left[\frac{h_2}{c}\ln(1 + \eta_i) + \ln(1 + \eta_i - \alpha\eta_i) \right] \tag{8a}$$

where:

$$\frac{h_2}{c} = \frac{1 - \alpha}{M_{ex} - 1} \tag{8b}$$

$$M_{ex} = \left[1 + 1.4\frac{\alpha\eta_i}{(1 + \eta_i)\Phi^2} \right]^{\frac{1}{2}} \tag{8c}$$

References

[1] Zerbst U, Madia M. Analytical flaw assessment. Engng Fract Mech 2018;187:316–67.
[2] BSi, BS 7910:2013 + A1 (incorporating corrigenda 2) - Guide to methods for assessing the acceptability of flaws in metallic structures. BSi; 2013.

[3] EDF, R6: Assessment of the integrity of structures containing defects, revision 4, Amendment 11. EDF Energy, Gloucester, 2015.
[4] Abaqus/CAE v6.12. Providence, RI, USA: Dassault Systemes Simulia Corp., 2012.
[5] FEACrack: 3D finite element software for cracks - user's manual. Quest integrity; 2015.
[6] Zencrack user manual, Issue 8.3," Zentech International Ltd.; 2018.
[7] FRANC3D reference manual, Version 7.3. Fracture analysis consultants, Inc.; 2018.
[8] Mi Y, Aliabadi MH. Dual boundary element method for three-dimensional fracture mechanics analysis. Engng Anal Boundary Elem 1992;10:161–71.
[9] Portela A, Aliabadi MH, Rooke DP. Dual boundary element incremental analysis of crack propagation. Comput Struct 1993;46(2):237–47.
[10] Citarella R, Lepore M, Fellinger J, Bykov V, Schauer F. Coupled FEM-DBEM method to assess crack growth in magnet system of Wendelstein 7-X. Frattura ed Integrità Strutturale 2013;26:92–103.
[11] Azuma K, Li Y, Hasegawa K. Characterization of interaction between elliptical subsurface flaws. In: Proceedings of the ASME 2016 pressure vessels and piping conference; 2016, no. 63429.
[12] Azuma K, Li Y. Interaction factors for two elliptical embedded cracks with a wide range of aspect ratios. AIMS Mater Sci 2017;4(2):328–39.
[13] Bezensek B, Sharples J. Flaw interaction rules given in BS 7910:2013 – The history and the way forward. Int J Press Vessels Pip 2018;168:225–32.
[14] Samadian K, Hertele S, Waele WD. Effects of flaw shape (idealization) on the interaction of co-planar surface flaws. In: Proceedings of the ASME 2018 pressure vessels and piping conference; 2018, no. 84506.
[15] Hasegawa K, Miyazaki K. Alignment and combination rules on multiple flaws in fitess-for-service procedures. In: 10th international conference on the mechanical behavior of materials, May 27-31, 2007, BEXCO, Busan, Korea; 2007. p. 411–6.
[16] Sethuraman R, Ilango IT. Analysis of interacting semi-elliptical surface cracks in finite thickness plates under remote bending load. Int J Press Vessels Pip 2005;82(7):528–45.
[17] Thomas RN, Paluszny A, Zimmerman RW. Quantification of fracture interaction using stress intensity factor variation maps. J Geophys Res: Solid Earth 2017;122(10):7698–717.
[18] Yoshimura S, Lee J-S, Yagawa G. Automated system for analyzing stress intensity factors of three-dimensional cracks: Its application to analyses of two dissimilar semi-elliptical surface cracks in plate. J Pressure Vessel Technol, Trans ASME 1997;119(1):18–26.
[19] Coules HE. On predicting the interaction of crack-like defects in ductile fracture. Int J Press Vessels Pip 2018;162:98–101.
[20] Coules HE. Flaw interaction under bending, residual stress and thermal shock loading. Procedia Struct Integrity 2018;13:361–6.
[21] Coules HE. Interaction of surface cracks subjected to non-uniform distributions of stress. Int J Press Vessels Pip 2017;157:20–9.
[22] Coules HE. Stress intensity interaction between dissimilar semi-elliptical surface cracks. Int J Press Vessels Pip 2016;146:55–64.
[23] Coules HE, Orrock PJ, Truman CE. Parametric design of scaled-down pressurised thermal shock test specimens using inelastic analysis. Engng Fract Mech 2017;176:308–25.
[24] MATLAB®, version 9.4.0.813654 (R2018a). Natick, USA: The Mathworks Inc.
[25] Abaqus/Standard v6.12. Providence, RI, USA: Dassault Systemes Simulia Corp., 2012.
[26] Shih CF, Moran B, Nakamura T. Energy release rate along a three-dimensional crack front in a thermally stressed body. Int J Fract 1986;30(2):79–102.
[27] Shih CF, Asaro RJ. Elastic-plastic analysis of cracks on bimaterial interfaces: Part 1 - Small scale yielding. J Appl Mech, Trans ASME 1988;55(2):299–316.
[28] Miller AG. Review of limit loads of structures containing defects. Int J Press Vessels Pip 1988;32:197–327.
[29] MATLAB® parallel computing toolbox, R2018a. Natick, USA: The Mathworks Inc.
[30] González-Albuixech VF, Qian G, Sharabi M, Niffenegger M, Niceno B, Lafferty N. Integrity analysis of a reactor pressure vessel subjected to a realistic pressurized thermal shock considering the cooling plume and constraint effects. Engng Fract Mech 2016;162:201–17.
[31] Brownell LE, Young EH. Process equipment design. John Wiley & Sons; 1959.
[32] Hill R. The mathematical theory of plasticity. Oxford University Press; 1950.
[33] Lei Y. A review of limit load solutions for cylinders with axial cracks and development of new solutions. Int J Press Vessels Pip 2008;85:825–50.
[34] Ramberg W, Osgood WR. Description of stress-strain curves by three parameters. NACA, NACA-TN-902; 1943.
[35] SINTAP. Structural Integrity Procedure for Europe v1a. SINTAP collaboration; 1999.
[36] Bezensek B, Coules HE. Recent studies towards updating the BS7910 flaw interaction rule. Proceedings of the ASME 2018 pressure vessels and piping conference. 2018.
[37] Bezensek B, Coules H, Sharples J, Tkach Y. Proposed updates to the buried-to-surface flaw transition rules in the Annex E of BS 7910. In: Proceedings of the ASME 2019 38th conference on ocean, offshore and arctic engineering, 2019, no. 96327.
[38] Coules HE, Bezensek B. Analysis of defect interaction in inelastic materials. In: Proceedings of the ASME 2019 pressure vessels & piping conference, 2019, no. PVP2019–93219.
[39] Newman JC, Raju IS. Analyses of surface cracks in finite plates under tension or bending loads. NASA 1979;1578.
[40] Merkle JG. A review of some of the existing stress intensity factor solutions for part-through surface cracks. Oak Ridge National Laboratory; 1973. ORNL-TM-3983.
[41] Lei Y. J-integral and limit load analysis of semi-elliptical surface cracks in plates under bending. Int J Press Vessels Pip 2004;81:31–41.
[42] Isida M, Noguchi H, Yoshida T. Tension and bending of finite thickness plates with a semi-elliptical surface crack. Int J Fract 1984;26(3):157–88.
[43] Newman JC, Raju IS. An empirical stress-intensity factor equation for the surface crack. Engng Fract Mech 1981;15(1–2):185–92.
[44] Raju IS, Newman JC. Stress-intensity factors for a wide range of semi-elliptical surface cracks in finite-thickness plates. Engng Fract Mech 1979;11(4):817–29.
[45] Paris PC, Sih GC. Stress Analysis of Cracks. In: Fracture tougness testing and its applications (ASTM STP381-EB); 1965.
[46] Shah RC, Kobayashi AS. Stress intensity factors for an elliptical crack approaching the surface of a semi-infinite solid. Int J Fract 1973;9(2):133–46.
[47] Kobayashi AS, Moss WL. Stress intensity magnification factors for surface-flawed tension plate and notched round tension bar. Proceedings of the second international conference on fracture. 1969. p. 31–40.
[48] Anderson RB, Holms AG, Orange TW. Stress intensity magnification for deep surface cracks in sheets and plates. NASA, TN D-6054; 1970.
[49] Smith FW, Sorensen DR. Mixed mode stress intensity factors for semi-elliptical surface cracks. NASA, CR-134684; 1974.
[50] Kobayashi AS. A simple procedure for estimating stress intensity factors in regions of high stress gradient. Proceedings of the 2nd international conference on mechanical behaviour of materials. 1976. p. 1073–7.
[51] Li R, Gao Z, Lei Y. A global limit load solution for plates with embedded off-set elliptical cracks under combined tension and bending. J Pressure Vessel Technol 2012;134(011204).
[52] Wells DN, Allen PA. Analytical round robin for elastic-plastic analysis of surface cracked plates: Phase I results. NASA, NASA/TM-2012-217456; 2012.